Langmuir
Article
pubs.acs.org/Langmuir

Fabrication of Highly Ordered TiO_2 Nanorod/Nanotube Adjacent Arrays for Photoelectrochemical Applications

Haimin Zhang,[†] Porun Liu,[†] Xiaolu Liu,[‡] Shanqing Zhang,[†] Xiangdong Yao,[†] Taicheng An,[‡] Rose Amal,[§] and Huijun Zhao*,[†]

[†]*Environmental Futures Centre and Griffith School of Environment, Gold Coast Campus, Griffith University, QLD 4222, Australia,* [‡]*State Key Laboratory of Organic Geochemistry, Guangzhou Institute of Geochemistry, Chinese Academy of Sciences, Guangzhou 510640, P. R. China, and* [§]*ARC Centre for Functional Nanomaterials, School of Chemical Sciences and Engineering, The University of New South Wales, NSW 2052, Sydney, Australia*

Received February 5, 2010. Revised Manuscript Received March 31, 2010

This work reports a facile approach to fabricate a perpendicularly aligned and highly ordered TiO_2 nanorod/nanotube (NR/NT) adjacent film by directly anodizing a modified titanium foil. The titanium foil substrate was modified with a layer of crystalline TiO_2 film via a hydrothermal process in 0.05 M $(NH_4)_2S_2O_8$. The resultant NR/NT architecture consists of a highly ordered nanorod top layer that directly adjoins to a highly ordered nanotube array bottom layer. The thickness of the top nanorod layer was ~90 nm with average nanorod diameter of 22 nm after 20 min of anodization. The thickness of the bottom nanotube array layer was found to be ca. 250 nm after 20 min of anodization, having an average outer and inner tubular diameters of 120 and 80 nm, respectively. A broad implication of the method is that a simple modification to the substrate surface can lead to new forms of nanostructures. For as-anodized NR/NT samples, XRD analysis reveals that the nanorods are of anatase TiO_2 crystalline form while the nanotubes are amorphous. Anatase TiO_2 crystalline form of NR/NT film with high crystallinity can be obtained by thermally treating the as-anodized sample at 450 °C for 2 h in air. The resultant NR/NT film was used as a photoanode for photoactivity evaluation. Comparing with a nanotube array photoanode prepared by direct anodization of unmodified titanium foil, the NR/NT photoanode exhibits a unique feature of selective photocatalytic oxidation toward organics, which makes it very attractive to photocatalytic degradation of organic pollutants, sensing, and other applications.

Introduction

Over the past decade, the nanotubular forms of titanium dioxide (TiO_2) have appealed to multidisciplinary fields due to their enormous potentials for photocatalysis,[1] sensing,[2] biomedicine,[3] and photovoltaic applications.[4−6] Numerous methods have been reported for fabricating TiO_2 nanotubes including template-assisted,[7] hydrothermal,[8] seed growth,[9] and anodization methods.[10] Among these synthetic methods, the anodization methods have shown outstanding performance in obtaining highly ordered TiO_2 nanotube arrays with controllable dimensions.[11−13] Such a form of highly ordered TiO_2 nanotube arrays have generated great interests for analytical,[14,15] photocatalytic,[16−18] and solar energy conversion applications.[4−6,19] It has been reported that the highly ordered TiO_2 nanotube arrays can remarkably increase the efficiency of water splitting and dye-sensitized solar cells.[4,16,17] A number of studies have demonstrated that the performance of TiO_2 nanotube arrays for dye-sensitized solar cells, and photocatalysis can be improved by alternating the structural and dimensional parameters of the array.[4,16−18] Schmuki et al. have alternated the architectures of TiO_2 nanotubes by adjusting anodization conditions to produce smooth nanotubes,[20] bamboo-type nanotubes,[21] and double-walled nanotubes.[22] These nanotubes show excellent potentials

*Corresponding author: Fax 61 7 55528067, Tel 61 7 55528261, e-mail h.zhao@griffith.edu.au.

(1) Mor, G. K.; Varghese, O. K.; Wilke, R. H. T.; Sharma, S.; Shankar, K.; Latempa, T. J.; Choi, K.-S.; Grimes, C. A. *Nano Lett*. **2008**, *8*, 1906–1911.
(2) Yoriya, S.; Prakasam, H. E.; Varghese, O. K.; Shankar, K.; Paulose, M.; Mor, G. K.; Latempa, T. J.; Grimes, C. A. *Sens. Lett*. **2006**, *4*, 334–339.
(3) Song, Y.-Y.; Schmidt-Stein, F.; Bauer, S.; Schmuki, P. *J. Am. Chem. Soc*. **2009**, *131*, 4230–4232.
(4) Kim, D.; Ghicov, A.; Albu, S. P.; Schmuki, P. *J. Am. Chem. Soc*. **2008**, *130*, 16454–16455.
(5) Shankar, K.; Mor, G. K.; Prakasam, H. E.; Varghese, O. K.; Grimes, C. A. *Langmuir* **2007**, *23*, 12445–12449.
(6) Wang, J.; Lin, Z. *Chem. Mater*. **2009**, *22*, 579–584.
(7) Lakshmi, B. B.; Patrissi, C. J.; Martin, C. R. *Chem. Mater*. **1997**, *9*, 2544–2550.
(8) Kasuga, T.; Hiramatsu, M.; Hoson, A.; Sekino, T.; Niihara, K. *Langmuir* **1998**, *14*, 3160–3163.
(9) Yue, L.; Gao, W.; Zhang, D.; Guo, X.; Ding, W.; Chen, Y. *J. Am. Chem. Soc*. **2006**, *128*, 11042–11043.
(10) Gong, D.; Grimes, C. A.; Varghese, O. K.; Hu, W.; Singh, R. S.; Chen, Z.; Dickey, E. C. *J. Mater. Res*. **2001**, *16*, 3331–3334.
(11) Ghicov, A.; Schmuki, P. *Chem. Commun*. **2009**, 2791–2808.
(12) Mor, G. K.; Varghese, O. K.; Paulose, M.; Shankar, K.; Grimes, C. A. *Sol. Energy Mater. Sol. Cells* **2006**, *90*, 2011–2075.
(13) Wang, D.; Liu, Y.; Yu, B.; Zhou, F.; Liu, W. *Chem. Mater*. **2009**, *21*, 1198–1206.
(14) Zhao, H.; Jiang, D.; Zhang, S.; Catterall, K.; John, R. *Anal. Chem*. **2004**, *76*, 155–160.
(15) Zheng, Q.; Zhou, B.; Bai, J.; Li, L.; Jin, Z.; Zhang, J.; Li, J.; Liu, Y.; Cai, W.; Zhu, X. *Adv. Mater*. **2008**, *20*, 1044–1049.
(16) Mor, G. K.; Shankar, K.; Paulose, M.; Varghese, O. K.; Grimes, C. A. *Nano Lett*. **2005**, *5*, 191–195.
(17) John, S. E.; Mohapatra, S. K.; Misra, M. *Langmuir* **2009**, *25*, 8240–8247.
(18) Allam, N. K.; Grimes, C. A. *Langmuir* **2009**, *25*, 7234–7240.
(19) Mor, G. K.; Shankar, K.; Paulose, M.; Varghese, O. K.; Grimes, C. A. *Nano Lett*. **2006**, *6*, 215–218.
(20) Macak, J. M.; Tsuchiya, H.; Taveira, L.; Aldabergerova, S.; Schmuki, P. *Angew. Chem., Int. Ed*. **2005**, *44*, 7463–7465.
(21) Albu, S. P.; Kim, D.; Schmuki, P. *Angew. Chem., Int. Ed*. **2008**, *47*, 1916–1919.
(22) Albu, S. P.; Ghicov, A.; Aldabergenova, S.; Drechsel, P.; LeClere, D.; Thompson, G. E.; Macak, J. M.; Schmuki, P. *Adv. Mater*. **2008**, *20*, 4135–4139.

in photovoltaic cells and membrane filtration applications.[4,22,23] It has been a general consensus that the mechanistic basis of the efficiency enhancement can be attributed to the effective electron percolation pathway provided by the perpendicularly aligned and highly ordered nanotubular architecture.[24−26] Grimes and co-workers reported that the electron transport conditions can be dramatically improved in the case of perpendicularly aligned and highly ordered TiO_2 nanotube arrays, as such an architecture facilitates vectorial charge transfer from the solution to the conducting substrate.[25] Moreover, their studies also demonstrate that the highly ordered TiO_2 nanotube arrays can possess high charge carrier densities after electrochemical doping.[27] Schmuki and co-workers have carried out a detailed study on the transport, trapping, and back-transfer of electrons in the highly ordered TiO_2 nanotube arrays.[28] They reported that the electron diffusion length in the TiO_2 nanotube arrays is on the order of 100 μm. Frank and co-workers recently revealed further insightful evidence by quantitatively measuring the charge transport and recombination time constants of both nanoparticulate and nanotubular TiO_2 films.[29] Their studies reveal that the recombination of charge carriers in a highly ordered nanotubular film is 10 times slower than that in a disordered nanoparticulate film, attributing to the improved charge collection efficiency and photoefficiency of TiO_2 nanotube electrode.[29] Despite these excellent achievements, the anodization has been almost exclusively carried out by directly anodizing unmodified titanium metal plate under various anodization conditions and supporting electrolyte compositions.[11,12] Under such conditions, the perpendicularly aligned TiO_2 nanotube arrays are the exclusive form of products.[11,12] It is well-known that the resultant nanostructures depend on starting materials.[30,31] It is therefore feasible to obtain different nanoarchitectures via anodization by employing premodified metal substrate, which would undoubtedly extend the capacity of anodization technique, leading to new nanoarchitectures suitable for various applications.

Herein we report a facile anodization method employing a modified titanium foil substrate to fabricate a novel nanoarchitecture with a perpendicularly aligned and highly ordered TiO_2 nanorod/nanotube (NR/NT) adjacent arrays structure. The photoelectrocatalytic performance of the resultant NR/NT photoanodes toward water and organic compounds was evaluated. To our best knowledge, this novel NR/NT adjacent arrays nanostructure has never been reported in the literature.

Experimental Section

Chemicals and Materials. Titanium (Ti) foils (0.25 mm thick, 99.7% purity) were supplied by Aldrich Corp. Hydrofluoric acid (HF, 48%), ammonium persulfate ($(NH_4)_2S_2O_8$, ≥98%), acetone, 2-propanol, and methanol (analytical grade) were purchased from Sigma-Aldrich without further treatment prior to use. High-purity deionized water (Millipore Corp., 18 MΩ cm) was used for the electrolyte solution preparation and the rinse of Ti substrates.

Fabrication. Titanium (Ti) foils (50 mm × 15 mm) were first degreased prior to use by sonication in acetone, 2-propanol, and methanol, subsequently rinsed with Milli-Q water, and finally dried in a nitrogen stream.[20] The pretreatment Ti foils were then placed in an autoclave containing 50 mL of 0.05 M $(NH_4)_2S_2O_8$ solution. The hydrothermal reaction was carried out at 120 °C for 1 h to obtain crystalline TiO_2 modification film.[32] The modified Ti foils were thoroughly washed with Milli-Q water and dried in a nitrogen stream. To obtain TiO_2 NR/NT adjacent nanostructure, the modified Ti foils were subjected to an anodization process under 20 V of applied voltage in 0.5% (v/v) HF electrolyte. All anodization experiments were carried out using a conventional power supply (dc power, MP-3084) with a titanium foil with crystalline TiO_2 film as anode and platinum mesh as cathode. After anodization, the samples were immediately removed from the reactor, rinsed with Milli-Q water, and then dried in a N_2 stream. The anodized samples were subsequently annealed in air at 450 °C for 2 h with heating and cooling rates of 2 °C/min to improve the mechanical strength and photocatalytic activity. For comparative experiments, the normal nanotube array (NT) films were prepared by direct anodization of unmodified Ti foil (the pretreatment Ti foil) under 20 V of applied voltage in 0.5% (v/v) HF electrolyte for 20 min. Both NR/NT and NT photoanodes were fabricated by incorporating the resultant TiO_2 NR/NT or NT film into a special electrode holder with 0.785 cm^2 exposed area for reaction.[26]

Characterization. SEM and TEM images of the samples were obtained using a JEOL JSM-6300F field emission scanning electron microscopy and FEI Tecnai 20 transmission electron microscopy, respectively. XRD patterns of the samples were obtained using a Shimadzu XRD-6000 diffractometer equipped with a graphite monochromator. Cu Kα radiation (λ = 1.5418 Å) and a fixed power source (40 kV and 40 mA) were used.

Measurements. The total concentration of titanium species in reaction solution under different anodization time was determined by a spectrophotometric method.[33] For each sample, the UV−vis spectroscopy was recorded from 190 to 800 nm using a Shimadzu UV 1691 spectrophotometer. The absorbance at 410 nm was used to quantify the total titanium concentration.[33] The photoelectrochemical measurements were performed at 23 °C in a photoelectrochemical cell with a quartz window for illumination.[34] It consisted of a TiO_2 NR/NT or a NT photoanode, a saturated Ag/AgCl reference electrode, and a platinum mesh counter electrode. A voltammograph (CV-27, BAS) was used for the application of potential bias. Potential and current signals were recorded using a Macintosh (AD Instruments). The illuminated area of the photoanode was 0.785 cm^2. All experiments were carried out in a 0.10 M $NaNO_3$ electrolyte solution with or without organics (i.e., 50 mM glucose). A 150 W xenon arc lamp light source with focusing lenses (HF-200W-95, Beijing Optical Instruments) was used as the illumination source. A UV bandpass filter (UG 5, Avotronics Pty. Ltd.) was employed to prevent the electrolyte from being heated by the infrared light. The light intensity was regulated and carefully measured at 365 nm.

Results and Discussion

The anodization methods reported to date have almost exclusively employed an unmodified Ti metal substrate to produce perpendicularly aligned TiO_2 nanotube arrays under various anodization conditions and supporting electrolyte compositions.[11,12] This work employed a modified Ti foil as the substrate for anodization to produce a NR/NT adjacent nanostructure. The modification

(23) Wang, J.; Lin, Z. *Chem. Mater.* **2008**, *20*, 1257–1261.
(24) Grimes, C. A. *J. Mater. Chem.* **2007**, *17*, 1451–1457.
(25) Paulose, M.; Shankar, K.; Varghese, O. K.; Mor, G. K.; Grimes, C. A. *J. Phys. D* **2006**, *39*, 2498–2503.
(26) Zhang, H.; Zhao, H.; Zhang, S.; Quan, X. *ChemPhysChem* **2008**, *9*, 117–123.
(27) Fabregat-Santiago, F.; Barea, E. M.; Bisquert, J.; Mor, G. K.; Shankar, K.; Grimes, C. A. *J. Am. Chem. Soc.* **2008**, *130*, 11312–11316.
(28) Jennings, J. R.; Ghicov, A.; Peter, L. M.; Schmuki, P.; Walker, A. B. *J. Am. Chem. Soc.* **2008**, *130*, 13364–13372.
(29) Zhu, K.; Neale, N. R.; Miedaner, A.; Frank, A. J. *Nano Lett.* **2007**, *7*, 69–74.
(30) Nah, Y.-C.; Ghicov, A.; Kim, D.; Schmuki, P. *Electrochem. Commun.* **2008**, *10*, 1777–1780.
(31) Wei, W.; Macak, J. M.; Schmuki, P. *Electrochem. Commun.* **2008**, *10*, 428–432.
(32) Allam, N. K.; Shankar, K.; Grimes, C. A. *Adv. Mater.* **2008**, *20*, 3942–3946.
(33) Lundell, G. E. F.; Hoffman, J. I.; Bright, H. A. *Chemical Analysis of Iron and Steel*; John Wiley & Sons: New York, 1931.
(34) Jiang, D.; Zhao, H.; Zhang, S.; John, R. *J. Catal.* **2004**, *223*, 212–220.

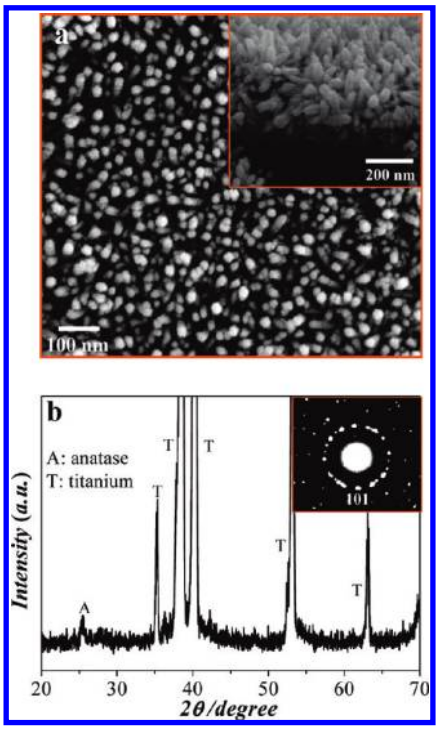

Figure 1. Surface SEM image (a) and X-ray diffraction pattern (b) of the modification layer via a hydrothermal process at 120 °C for 1 h in 0.05 M $(NH_4)_2S_2O_8$ solution. Inset in (a): cross-sectional SEM image of crystalline TiO_2 modification film. Inset in (b): SAED pattern of individual nanorod.

was carried out via a hydrothermal process in a reaction solution containing 0.05 M $(NH_4)_2S_2O_8$ at 120 °C for 1 h. Figure 1a shows the surface and cross-section SEM images of the resultant modification film. The top layer of the modified film is covered by high density nanorods, having an average length and diameter of 90 and 30 nm, respectively. The cross-section SEM image (inset in Figure 1a) of the modification film reveals an asymmetric structure consisting of a 90 nm nanorod top layer and a 220 nm porous nanoparticle bottom layer. Most nanorods are perpendicularly grown but are not in a highly ordered form. Figure 1b shows the X-ray diffraction (XRD) pattern of the modification film, indicating that the modification film is dominated by anatase TiO_2. The selected-area electron diffraction (SAED) pattern (inset in Figure 1b) suggests that the modified film possesses a relatively high crystallinity.

The modified Ti foil was then employed as the substrate and subjected to an anodization process under a constant applied voltage of 20 V for 20 min in 0.5% (v/v) HF electrolyte. Figure 2 shows SEM images of resultant film after anodization. The image shown in Figure 2a demonstrates a nanorod arrays surface layer with an average nanorod diameter of ~22 nm. The SAED pattern (inset in Figure 2a) of individual nanorod shows similar crystallinity as the modification film. In an attempt to obtain the cross-section structure of the resultant film, we surprisedly discovered that the resultant film is formed by a nanorod/nanotube adjacent array structure (see Figure 2b). A highly ordered nanorod arrays top layer with ~90 nm in thickness is directly adjoined to a highly ordered nanotube arrays bottom layer. Before annealing, the two layers can be readily separated by high strength adhesive tape. Figure 2c shows SEM image of the nanotube arrays layer underneath the nanorod layer. These nanotubes possess an average outer diameter of 120 nm and an inner diameter of 80 nm. The cross-section image reveals a 250 nm average tube length

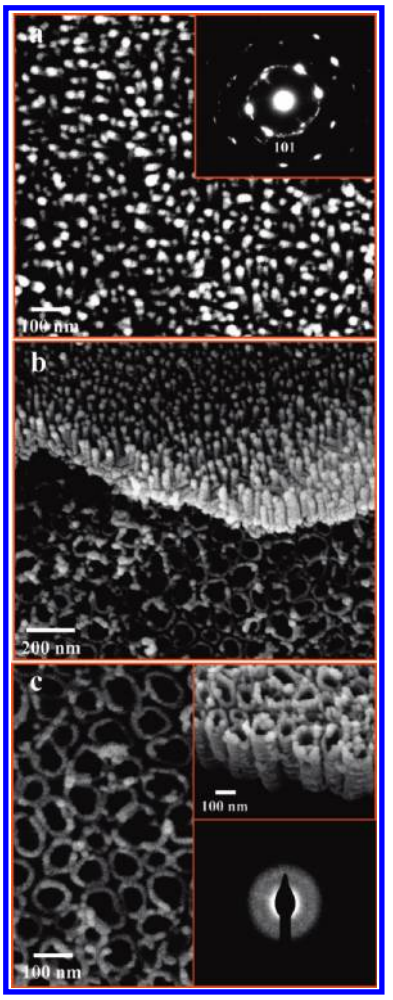

Figure 2. SEM images of as-anodized TiO_2 nanorod/nanotube adjacent structure fabricated by anodization of titanium foil modified with crystalline TiO_2 film at 20 V for 20 min in 0.5% (v/v) HF solution. Surface SEM image of top TiO_2 nanorod arrays with inset of SAED pattern of individual nanorod (a), SEM image of TiO_2 nanorod/nanotube adjacent structure (b), and SEM image of the nanotube arrays underneath the nanorod arrays with the top inset of cross-sectional SEM image of the underneath nanotube arrays and the bottom insert of SAED pattern of individual nanotube (c).

(top inset in Figure 2c). XRD analysis was used to examine the crystalline phase of the as-anodized NR/NT film. The XRD pattern of the as-anodized NR/NT film shows the characteristics of anatase TiO_2 crystalline (curve a in Figure 3). Considering the asymmetric NR/NT structure of the as-anodized film, the anatase TiO_2 crystalline characteristics observed from the XRD analysis is likely due to the nanorod top layer (see Figure 1b) because a well-known fact that the as-anodized nanotubes without thermal treatment are amorphous (see curve b in Figure 3).[11,12] It is to note that the XRD pattern shown in the curve b in Figure 3 was obtained from a nanotube arrays sample prepared by direct anodization of unmodified Ti foil under the same conditions as for the sample used to obtain the curve a in Figure 3. In order to confirm this, the nanorod top layer of a NR/NT sample was removed to expose the underneath nanotubes. The SAED pattern of the underneath nanotube (bottom inset in Figure 2c) confirms that these nanotubes are amorphous. The as-anodized NR/NT samples were subjected to a thermal treatment process at 450 °C in air for 2 h to improve the mechanical strength and crystallinity. The XRD analysis reveals that these thermally treated NR/NT samples show a dramatically improved crystallinity with anatase

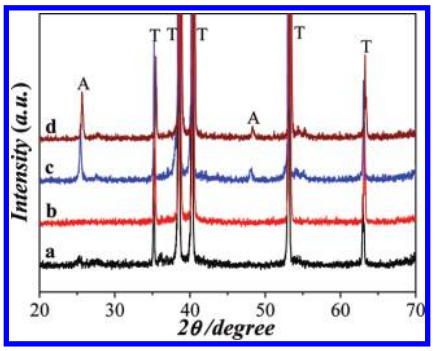

Figure 3. X-ray diffraction patterns of as-anodized TiO_2 NR/NT sample (curve a), as-anodized TiO_2 nanotube sample obtained from direct anodization of unmodified Ti foil (curve b), TiO_2 NR/NT sample annealed at 450 °C for 2 h (curve c), and the underneath TiO_2 nanotube array layer annealed at 450 °C for 2 h (curve d). A: anatase; T: titanium.

TiO_2 as the dominated phase (curve c in Figure 3). This suggests that a 450 °C thermal treatment temperature is sufficient to convert the underneath amorphous nanotubes into crystalline anatase TiO_2 nanotubes. In order to further confirm this, a underneath nanotubular sample was prepared and thermally treated at 450 °C in air for 2 h for XRD analysis. The obtained XRD pattern confirms that the underneath amorphous nanotubes were converted to anatase TiO_2 nanotubes with high crystallinity (curve d in Figure 3). It should be noted that the SEM analysis of the thermally treated samples at 450 °C was also conducted. No observable effect of thermal treatment on the morphology and the NR/NT adjacent structure was found (the SEM images are not shown).

The NR/NT adjacent structure formation process was investigated by SEM analysis of resultant nanostructures under different anodization time and measurement of the titanium source concentration in reaction solution at the corresponding anodization time (see Figure 4). Figure 4a shows a typical SEM image of the resultant film after 5 min of anodization under 20 V of applied voltage. It reveals a perpendicularly grown nanorod top layer similar to the top layer morphology of the modification film (inset in Figure 1a). The top layer is found to be ~250 nm, consisting of an ~100 nm nanorod layer and a 150 nm porous nanoparticle layer (top inset in Figure 4a). Comparing to the original modification film, a noticeable improvement on the order of the nanorods alignment can be observed. The average length of the nanorods increases slightly to 100 nm while the average diameter of the nanorods is decreased from 30 to 28 nm. However, the most noticeable change resulting from the anodization is the dramatically decreased porous nanoparticle layer thickness from 220 to 150 nm, suggesting a dominant dissolution process at this stage. The changes to the underneath layer are also observable. The infant forms of nanotubes start to appear (bottom inset in Figure 4a). With 10 min of anodization (Figure 4b), the SEM image reveals a further improved order of the top layer nanorods (top inset in Figure 4b). The average length of the nanorods is further increased to 120 nm and the average diameter of the nanorods is decreased slightly to 25 nm, while the porous nanoparticle layer thickness is reduced to ~50 nm. The rapid decreased porous nanoparticle layer thickness suggests that the dissolution process still dominates at this stage. For the underneath layer, the SEM analysis confirms a perpendicularly aligned and highly ordered nanotube array structure (bottom inset in Figure 4b). The resultant nanotubes possess average outer and inner diameters of approximately 120 and 80 nm, respectively.

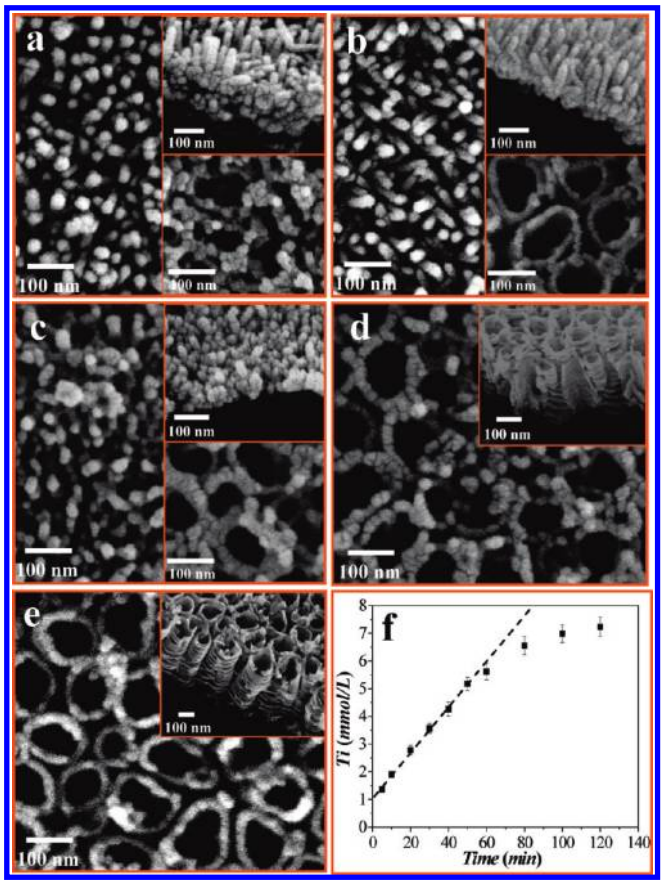

Figure 4. SEM images of TiO_2 samples anodized at 20 V in 0.5% (v/v) HF with various anodization times of 5 (a), 10 (b), 30 (c), 60 (d), and 80 min (e); the plot of the total concentration of Ti species in reaction solution against the anodization time (f). Insets in (a−c): cross-sectional SEM images of the top layer structure (top images) and surface SEM images of the underneath nanotube arrays (bottom images). Insets in (d, e): cross-sectional SEM images of nanotube arrays.

The cross-section image (not shown) reveals an average tube length of 200 nm. When a 20 min of anodization time was employed (see Figure 2), the SEM analysis reveals a perpendicularly aligned and highly ordered nanorod top layer structure while the nanoparticle layer disappears (Figure 2b). The average diameter, length, and density of nanotubes are found to be reduced when compares to the case of 10 min of anodization. The changes in dimensions, distribution density, and degree of alignment and order of the nanorods imply the occurrence of a reorganization process, though both the disappearance of nanoparticle layer and the reduced density of the nanorods suggest the domination of the dissolution process continues. The morphology as well as outer and inner diameters of the underneath nanotubes are similar to those obtained from 10 min anodized samples (Figure 2c). The surface morphology of the resultant film changes dramatically when the anodization time was increased to 30 min (Figure 4c). The highly ordered nanorod structure is reduced to a particle-like structure (top inset in Figure 4c), suggesting the domination of dissolution process continues. However, the changes in the outer and inner diameters of the underneath nanotubes are less obvious (bottom inset in Figure 4c), except the average length of the nanotubes is increased to 220 nm. After 60 min of anodization, the top nanorod layer is further reduced to a small amount of nanoparticles distributed on the surface of the nanotube array layer, and the NR/NT adjacent nanostructure

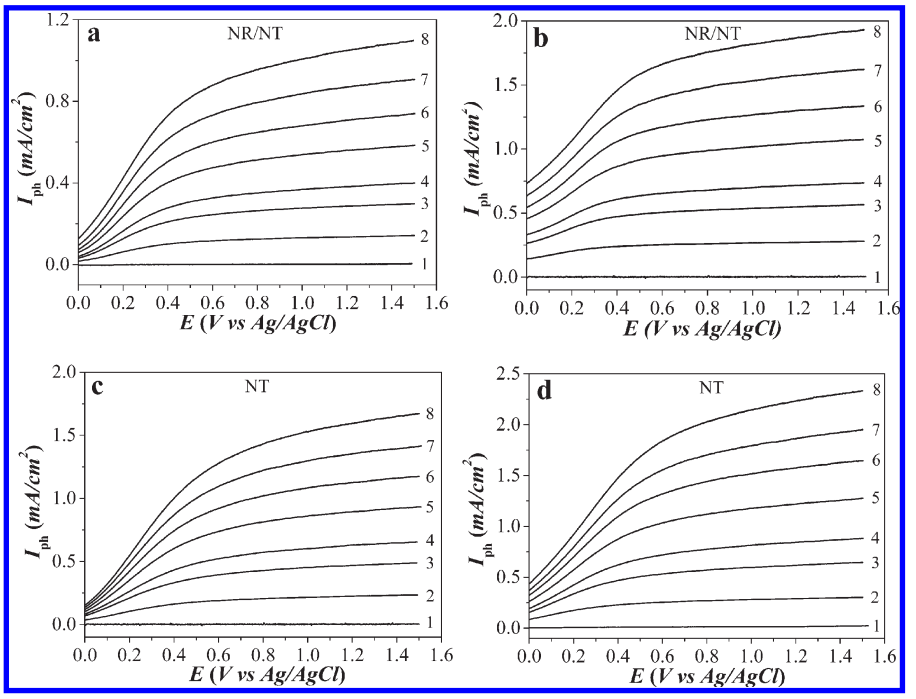

Figure 5. Voltammograms obtained under different light intensities from a NR/NT photoanode in 0.10 M $NaNO_3$ supporting electrolyte solution (a) and in the presence of 50 mM glucose (b) and from a NT photoanode in 0.10 M $NaNO_3$ supporting electrolyte solution (c) and in the presence of 50 mM glucose (d). Curve 1 in (a) to (d): without UV illumination; the light intensity of curves 2−8 in (a) to (d): 1.2, 2.5, 3.5 5.0, 6.5, 8.0, and 9.5 mW/cm^2.

becomes a single layer nanotube array (Figure 4d). The disappearance of the nanorod layer confirms the dissolution process still occurs. Compared to 30 min anodized nanotubes, these 60 min anodized nanotubes exhibit similar tubular dimensions, except an increased length to ca. 250 nm (inset in Figure 4d). Figure 4e shows the SEM image of the sample after 80 min of anodization. The resultant structure exhibits a typical nanotube array structure with similar tubular parameters including the tube length (inset in Figure 4e) to those shown in Figure 4d, except a cleaner tubular surface. For samples subjected to anodization time up to 120 min, the SEM analysis reveals similar nanotube array structure and tubular parameters as those of 60 min anodized samples. Figure 4f shows the plot of total titanium concentration in reaction solution against the anodization time. Such a concentration−time profile matches the structural changes revealed by SEM analysis. A linearly increased total titanium concentration with the anodization time up to 50 min is observed, corresponding to the dissolution of the top layer structures as shown in Figure 2 and Figures 4a−c. The concentration increase becomes less rapid with the anodization time greater than 60 min where the dissolution of the top layer structures nearly completes (Figure 4d). The total titanium concentration in solution reaches a semisaturated status when the anodization time is beyond 80 min due to the complete dissolution of the top layer structures (Figure 4e).

The mechanistic pathway for the formation of the NR/NT adjacent nanostructure was considered. Experimental results shown in Figures 1−3 confirm that the crystalline form of the nanorod top layer and the underneath nanotube array layer of the as-anodized NR/NT film are different. The nanorod top layer possesses a crystalline form of anatase TiO_2 similar to the modification layer, while the underneath nanotube arrays are amorphous, alike anodized nanotubes from unmodified Ti substrate without thermal treatment. This may imply that the nanorod top layer and the underneath nanotube array layer are formed via separated processes/mechanisms. It is well-known that HF is a highly corrosive reagent. The crystalline TiO_2 formed on the modified Ti foil substrate can be etched by HF to form H_2TiF_6 during anodization process, resulting in the dissolution of the crystalline TiO_2 (the forward reaction of eq 1).[35] At the same time, the produced H_2TiF_6 species can react with H_2O, forming TiO_2 seeds that aggregate/deposit on the substrate surface via a crystal growth process (the reverse reaction of eq 1).[35] The nanorod top layer can be formed via the deposition and reorganization of TiO_2 seeds during the dynamic chemical dissolution and deposition processes.

$$TiO_2(s) + 6HF \underset{\text{dissolution/reorganization and deposition}}{\longleftrightarrow} H_2TiF_6 + 2H_2O \quad (1)$$

Considering the porous structure of the modification film would allow HF in solution to reach the underneath Ti metal surface, the formation mechanism for the underneath nanotube array layer should be the same as those reported nanotube array formation mechanisms under the anodization conditions for unmodified Ti foil substrate.[11,12] The formation of anatase TiO_2 nanorod top layer may be independent of the formation of underneath amorphous nanotube arrays. Nevertheless, the anodization process may affect the chemical dissolution and deposition conditions, which in turn affect the formation of nanorod layer. A set of comparison experiments was therefore carried out to investigate the effect of anodization process on the nanorod layer formation. The crystalline TiO_2 modified substrates were subjected to HF treatments in the absence of anodization process (without applied anodic potential). Under such conditions, the crystalline TiO_2 modified layer shown in Figure 1a was rapidly dissolved and destroyed within 10 min of HF treatment, suggesting an accelerated dissolution process

(35) Wu, G.; Wang, J.; Thomas, D. F.; Chen, A. *Langmuir* **2008**, *24*, 3503–3509.

(Figures S1a and S1b in the Supporting Information). The growth of nanorods can be observed from a prolonged reaction time of 20 min (see Figure S1c in Supporting Information). However, the density of the nanorods was found to be low in comparison to those shown in Figure 2. These observations confirm the effect of anodization process on the formation of nanorod layer. It has been reported that high concentration of titanium species such as $[TiF_6]^{2-}$ can be produced during the anodization process, attributing to the field-assisted dissolution.[11,12] For this work, the anodization process could contribute to the formation of high density nanorods (see Figure 2) by providing high concentration titanium sources in solution that facilitates the chemical deposition (growth) process.

The photocatalytic activities of NR/NT nanostructure as photoanode toward photocatalytic oxidation of water and glucose were investigated (Figure 5). The NR/NT photoanode was fabricated by incorporating the thermally treated NR/NT adjacent film into a special electrode holder with a 0.785 cm^2 exposed area for reaction. Our experimental results demonstrated that no noticeable change in morphology was observed, indicating good thermal stability of TiO_2 NR/NT adjacent structure after thermal treatment at 450 °C for 2 h. Figure 5a shows the voltammograms of the NR/NT photoanode in 0.10 M $NaNO_3$ supporting electrolyte solution with or without UV illumination. Without UV illumination, only a negligible dark current was measured. For all cases with UV illumination, the photocurrents (I_{ph}) increase linearly as the applied potential bias increases within the low potential range, attributing to the limitation of free photoelectron transport within the TiO_2 catalyst film.[34,36] The photocurrents saturate at higher potentials due to the limitation of the interfacial processes at the catalyst/solution interface.[34,36−38] An increase in the light intensity leads to an increase in the saturated photocurrents (I_{sph}). The magnitude of I_{sph} represents the maximum rate of water oxidation under a given light intensity (φ).[36] The voltammograms of NR/NT photoanode in 0.10 M $NaNO_3$ containing 50 mM glucose with or without UV illumination are given in Figure 5b. These voltammograms are found to be qualitatively similar to those shown in Figure 5a for water oxidation, except the I_{sph} obtained in presence of organics (i.e., glucose) is higher than the I_{sph} obtained in absence of glucose under the same light intensity. For comparison, the photocatalytic activities of the nanotube arrays (NT) photoanode toward photocatalytic oxidation of water and glucose were evaluated. It should be noted that the nanotube arrays (NT) photoanodes were fabricated by direct anodization of unmodified Ti foil at 20 V of voltage for 20 min in 0.5% (v/v) HF solution. Figures 5c and 5d show the voltammograms of NT photoanode under identical experimental conditions as those used for Figures 5a and 5b, respectively. In terms of $I-E$ curve characteristics, these voltammograms are qualitatively similar to those shown in Figures 5a and 5b for NR/NT photoanode. In the case of water oxidation, it can be seen that the measured I_{sph} values under corresponding light intensities from the NT photoanode are higher than that obtained from the NR/NT photoanode (see Figures 5a,c). This suggests that the NT photoanode possesses a higher photoactivity toward water oxidation than that of the NR/NT photoanode. In the presence of glucose, similar conclusions can be drawn when compares the data shown in Figures 5b and 5d. However, the measured photocurrent in presence of glucose consists of two current components. One is due to the photocatalytic oxidation of water and the magnitude of this current component is essentially the same as the photocurrent obtained in absence of glucose under a corresponding light intensity (i.e., I_{sph} values presented in Figures 5a and 5c).[14,39] Another is contributed by the photocatalytic oxidation of glucose. As a result, the I_{sph} obtained in presence of glucose can be regarded as the overall saturation photocurrent. For this reason, the higher overall I_{sph} values observed from a NT photoanode in presence of glucose (as shown in Figure 5d) does not necessarily confirm the NT photoanode possesses a higher photocatalytic activity toward glucose oxidation than that of the NR/NT photoanode. This is because the measured increase in overall I_{sph} could be due to the higher water oxidation photocurrent component of the NT photoanode, as demonstrated in Figure 5c. A further analysis is therefore needed to precisely examine the photocatalytic characteristics of the two photoanodes. To achieve such a purpose, the I_{sph} values obtained from both photoanodes are plotted against the light intensities (φ) for photocatalytic oxidation of water and glucose (see Figures 6a and 6b).

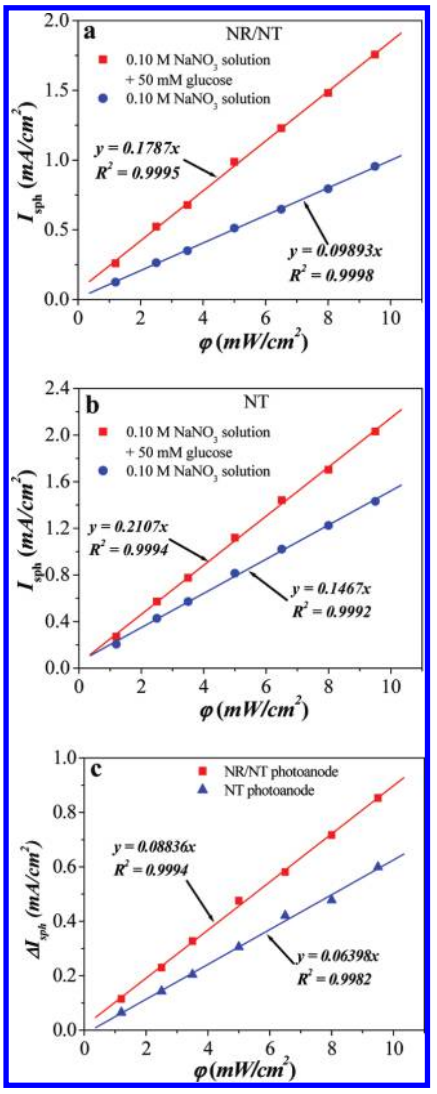

Figure 6. Relationships of saturation photocurrent with light intensity for NR/NT photoanode (a), for NT photoanode (b), and relationships of net saturation photocurrent with light intensity for NR/NT and NT photoanodes (c). The saturation photocurrent data were derived from $I_{ph}-E$ curves shown in Figures 5a−d at +0.80 V of applied potential.

(36) Jiang, D.; Zhao, H.; Zhang, S.; John, R. *J. Phys. Chem. B* **2003**, *107*, 12774–12780.
(37) Zhao, H.; Jiang, D.; Zhang, S.; Wen, W. *J. Catal.* **2007**, *250*, 102–109.
(38) Wen, W.; Zhao, H.; Zhang, S.; Pires, V. *J. Phys. Chem. C* **2008**, *112*, 3875–3880.
(39) Zhang, S.; Jiang, D.; Zhao, H. *Environ. Sci. Technol.* **2006**, *40*, 2363–2368.

The I_{sph} data used in Figures 6a and 6b were derived from $I_{ph}-E$ curves shown in Figures 5a to 5d at +0.80 V of applied potential bias. Well-defined linear $I_{sph}-\varphi$ relationships are obtained from all cases investigated. Under the given experimental conditions, the slope value of the $I_{sph}-\varphi$ curve quantitatively represents the photocatalytic activity of the photoanode. For NR/NT photoanode, the slope values of 0.098 93 mA/mW (R^2 = 0.9998) and 0.1787 mA/mW (R^2 = 0.9995) are obtained for photocatalytic oxidation of water and in presence of glucose, respectively (see Figure 6a). The former slope value quantifies the photoactivity of the photoanode toward photocatalytic oxidation of water, and the latter represents the overall photoactivity of the photoanode. With NT photoanode, the slope values are of 0.1467 mA/mW (R^2 = 0.9992) and 0.2107 mA/mW (R^2 = 0.9994) for photocatalytic oxidation of water and in presence of glucose, respectively (see Figure 6b). This means that for photocatalytic oxidation of water the slope of the NT photoanode is almost 1.5 times the slope value obtained from the NR/NT photoanode, which confirms the NT photoanode possesses a higher photoactivity toward water oxidation. Likewise, the slope of the NT photoanode in presence of glucose is nearly 1.2 times higher than the slope of the NR/NT photoanode, indicating a higher overall photocatalytic activity of the NT photoanode. In order to quantify the photoactivity toward glucose, the net photocurrent (ΔI_{sph}) is deducted from the saturation photocurrents of corresponding light intensity in the presence and absence of glucose for both photoanodes. The obtained ΔI_{sph} is due purely to the photocatalytic oxidation of organics (i.e., glucose).[14,39] Plotting ΔI_{sph} against φ gives straight lines with slope values of 0.088 36 mA/mW (R^2 = 0.9994) and 0.063 98 mA/mW (R^2 = 0.9982) for NR/NT and NT photoanodes, respectively (see Figure 6c). As the slope of a $\Delta I_{sph}-\varphi$ curve represents the photocatalytic activity of a photoanode toward organic oxidation, the data shown in Figure 6c imply that the photoactivity of the NR/NT photoanode toward glucose oxidation is near 1.4 times higher than that of the NT photoanode. In other words, the NR/NT photoanode possesses a characteristic of selective photocatalytic oxidation toward organics (i.e., glucose). Such a unique feature makes the NR/NT photoanode very attractive to applications such as environmental remediation and analytical determination of organic pollutants, where selective oxidation of organics is highly desirable.[14,15] It should be mentioned that the photocatalytic oxidation of other organic compounds such as methanol, ethanol, and sucrose were also performed. The photocatalytic oxidation characteristics of the photoanode obtained from these organic compounds were found to be qualitatively similar to those shown in Figures 5 and 6.

Conclusion

In summary, we have demonstrated a facile approach to fabricate a novel perpendicularly aligned and highly ordered TiO_2 nanorod/nanotube adjacent film on conducting substrate by directly anodizing a modified titanium foil. A broad implication of the method is that a simple modification to the substrate can lead to new forms of nanostructures. The resultant NR/NT photoanode demonstrates a unique feature of selective photocatalytic oxidation toward organics, which makes it very attractive to photocatalytic degradation of organic pollutants, sensing, and other applications.

Acknowledgment. This work was financially supported by Australian Research Council.

Supporting Information Available: Surface SEM images of the crystalline TiO_2 modified film after 0.5% HF treatment without applied anodic potential. This material is available free of charge via the Internet at http://pubs.acs.org.